Jambura Journal of Biomathematics

RESEARCH ARTICLE

Study on Listeriosis Transmission Dynamics including Time Lag and Media-Driven Behavioral Change

Kapil Toor[1], **and Kalyan Das**[1]

[1]Department of Interdisciplinary Sciences, National Institute of Food Technology Entrepreneurship and Management, HSIIDC Industrial Estate, Kundli - 131028, Haryana, India

Corresponding author. Email: *daskalyan27@gmail.com*

Article Identity
Jambura J. Biomath.
Volume 7 Issue 1 Pages 176 – 196
March 2026, E-ISSN 2723-0317

Article History
Received 18 November 2025
Revised 19 march 2026
Accepted 30 March 2026
Published 30 March 2026

Keywords
Listeriosis, Stability, Infectious disease, Delay, Hopf bifurcation, Sensitivity, Contaminated food

Editorial office: Department of Mathematics, Universitas Negeri Gorontalo, Jln. Prof. Dr. Ing. B. J. Habibie, Bone Bolango 96554, Indonesia

To Cite this Article: Toor K and Das K. Study on Listeriosis Transmission Dynamics including Time Lag and Media-Driven Behavioral Change. Jambura Journal of Biomathematics. 2026;7(1):176-196. doi:10.37905/jjbm.v7i1.25

Abstract. *Listeriosis is a foodborne disease caused by the bacterium Listeria monocytogenes, posing significant risks to public health due to its high mortality rate among vulnerable populations. This study develops a comprehensive mathematical model to analyze the dynamics of Listeriosis transmission, incorporating human populations, bacterial growth, food contamination, and the influence of media campaigns. The model divides the human population into compartments of unaware susceptible, aware susceptible, infected, and recovered individuals, while also tracking bacterial populations, media campaigns, and uncontaminated and contaminated food supplies. To capture realistic disease progression, the model includes a delay term τ to account for time lags in awareness campaigns and contamination processes. Stability analysis of the disease-free and endemic steady states is performed to identify critical thresholds for disease control. Additionally, the effects of delays on the system's stability and the potential for oscillatory dynamics are investigated. Sensitivity analysis is conducted to determine the influence of key parameters on disease dynamics. The model provides valuable insights into effective strategies for controlling Listeriosis and mitigating its impact on public health.*

1. Introduction

Mathematical modelling has become an important tool for understanding the transmission dynamics and control of infectious diseases. By formulating mathematical models, researchers can describe the mechanisms of disease spread, evaluate intervention strategies, and predict possible outbreak scenarios. Classical works in epidemiology laid the foundation for modern infectious disease modelling. In particular, the pioneering work of Kermack and McKendrick [1] introduced the compartmental modelling framework, which has since been widely used to study epidemic processes in human populations. Later developments by Anderson and May [2] further expanded the application of population biology principles to infectious disease dynamics.

An important concept in epidemiological modelling is the basic reproduction number, which determines whether an infectious disease can invade and persist in a population. The framework developed by Van den Driessche and Watmough [3] provides a systematic approach for calculating reproduction numbers and analyzing the stability of disease-free and endemic equilibria in compart-

mental models.

The theory of dynamical systems has also played a significant role in analyzing biological and epidemiological models. Concepts such as persistence, stability, and permanence provide insight into the long-term behavior of populations and disease transmission systems. Hutson and Schmitt [4] discussed the permanence and persistence of biological systems, which are important properties in determining whether a disease remains in a population over time. Similarly, Zhao [5] provided a comprehensive framework for studying dynamical systems in population biology, highlighting the mathematical techniques used to analyze stability and persistence in epidemiological models.

Listeriosis is a serious foodborne infection caused by the bacterium Listeria monocytogenes. Although relatively rare, it is associated with high hospitalization and mortality rates, particularly among pregnant women, newborns, elderly individuals, and immunocompromised patients. Studies such as those by Allerberger and Wagner [6] and Schlech and Acheson [7] have documented the clinical significance and epidemiology of foodborne listeriosis, emphasizing the need for effective control strategies. Recent public health reports, including those by the National Listeria Incident Management Team [8], highlight the ongoing concern regarding outbreaks linked to contaminated food products. Food contamination and cross-contamination play a critical role in the transmission dynamics of listeriosis. Ready-to-eat food products are particularly vulnerable to contamination during processing, storage, and handling. Chukwu and Nyabadza [9] developed a theoretical mathematical model that describes the spread of listeriosis through cross-contamination of ready-to-eat food products. Such models help to identify key factors influencing disease transmission and to evaluate possible intervention strategies.

Listeria monocytogenes represents one of the most significant foodborne pathogens of global concern, particularly due to its association with ready-to-eat (RTE) food products and its severe health implications for vulnerable populations [10]. The pathogenscan survive and reproduce under refrigeration conditions, combined with its widespread presence in food processing environments, makes it a persistent threat to public health [11]. In recent years, the increasing incidence of human invasive listeriosis, particularly in the European Union and European Economic Area, has highlighted the urgent need for comprehensive approaches to understanding and controlling this pathogen [12].

The complexity of listeriosis transmission dynamics extends beyond simple food contamination scenarios. Mathematical modeling approaches have emerged as powerful tools for understanding disease transmission patterns, with researchers developing sophisticated compartmental models that incorporate both human and animal populations [13]. These models have evolved to address not only single-pathogen scenarios but also coinfection dynamics, as demonstrated in studies examining the simultaneous occurrence of listeriosis and anthrax infections [14]. Such comprehensive modeling frameworks provide valuable insights into the interplay between different disease transmission pathways and help identify critical control points for intervention strategies.

Optimal control theory has been increasingly applied to listeriosis research, offering systematic approaches to identify the most effective intervention strategies. Studies have demonstrated that combined control measures, including media campaigns, treatment protocols, and removal of contaminated food products, are significantly more effective than individual interventions [15]. The application of cost-effectiveness analysis through concepts such as the Intervention Averted Ratio has further refined our understanding of resource allocation for maximum public health impact. These findings emphasize that treatment of both infected humans and animals represents the most effective strategy for controlling listeriosis transmission. The food safety dimension of listeriosis control has been extensively studied through quantitative microbial risk assessment (QMRA) approaches. Research on commercial meat products, such as salami in Southern Brazil, has revealed significant annual infection probabilities, with estimates reaching 98.1 percentage for Staphylococcus aureus, 71 percentage for Salmonella typhi, and 27 percentage for enteropathogenic Escherichia coli [16]. These findings underscore the limitations of traditional microbiological testing alone and support QMRA as an essential

complementary tool for food safety decision-making, particularly for traditionally produced fermented meat products.

International efforts toward harmonizing Listeria monocytogenes control strategies have emphasized the need for risk-based policies that incorporate input from all stakeholders across local and national levels. Expert consensus has been reached on microbiological criteria, though challenges remain for industry compliance and government assessment. The importance of robust testing regimes for food and food-contact surfaces, environmental monitoring, and the development of quantitative detection methods capable of identifying the pathogen at levels below $100 CFU/g$ has been consistently highlighted [17].

Predictive modeling has emerged as a critical tool for food safety management, with researchers developing and validating regression models for L. monocytogenes growth in specific food products. Studies on roast beef have identified storage temperature, sodium lactate and packaging interactions as significant predictors of pathogen growth with temperature being the most influential factor [18]. Advanced stochastic models have been developed for naturally contaminated lightly preserved seafood, demonstrating the crucial importance of lag time and microbial interactions in accurate growth predictions [19]. These models have shown that without considering these factors, unrealistically high maximum population density values may be predicted, potentially leading to inappropriate risk assessments.

The epidemiological context of listeriosis continues to evolve, with particular concern for vulnerable populations including the elderly pregnant women and individuals with weak immunity. European surveillance data indicate that more than 90 percentage of invasive listeriosis cases are linked to the ingestion of RTE food containing greater than 2,000 CFU/g, with approximately one-third of cases attributed to pathogen growth during the consumer phase [12]. Regional risk assessment studies have demonstrated that cooked ham products pose the highest risk among RTE products, while effective control measures such as reduced storage temperature and time can significantly decrease listeriosis risk [20].

The integration of mathematical modeling, optimal control theory, predictive microbiology, and risk assessment represents a comprehensive approach to understanding and controlling listeriosis. This multidisciplinary framework provides the foundation for developing evidence-based strategies that can effectively reduce the burden of listeriosis while optimizing resource allocation for maximum public health benefit. As the complexity of food systems continues to increase and vulnerable populations grow, such integrated approaches become increasingly essential for protecting public health from this persistent foodborne pathogen.

Motivated by these studies [21–25], the present work focuses on the development and analysis of a mathematical model describing the transmission dynamics of listeriosis with particular emphasis on contamination mechanisms and media awareness effects. The model incorporates different population compartments along with bacterial and food contamination dynamics. Mathematical analysis including positivity, boundedness, equilibrium analysis, and stability investigation is performed to better understand the long-term behavior of the system and the impact of various parameters on disease control.

The organization of this paper is as follows. Section 2 presents the formulation of the proposed mathematical model along with the model assumptions, state variables, and parameter descriptions. Sections 3 to 5 establishes the fundamental properties of the model, including the positivity, boundedness, and permanence of solutions. In Section 6, steady State Analysis is carried out with all possible equilibrium points of the system and their existence conditions are derived. Section 7 consists of the local stability of the equilibrium points of the delay-free system is analyzed using the Jacobian matrix and eigenvalue criteria. The global stability of the equilibrium states is investigated in Section 8 using appropriate Lyapunov functions. The model is extended by incorporating time delay, and the effects of delay on the system dynamics are examined Section 9. Conditions for the occurrence of

Hopf bifurcation and stability switching due to time delay are derived in Section 10. Sensitivity analysis is performed in Section 11, to identify the parameters that significantly influence the transmission dynamics. Numerical simulations are carried out to illustrate and support the theoretical results in Section 12. The main findings of the study are summarized and their biological implications are discussed in Section 13, along with possible directions for future research.

2. Formulation of Listeriosis Model

The Listeriosis model is governed by the following system (1) of differential equations and the corresponding state variables and parameters are described in Table 1.

$$\begin{aligned}
\frac{dS_1}{dt} &= r_1N + r_2S_4 + r_3S_2 - \lambda_1S_1 - r_5M(t-\tau)S_1(t-\tau),\\
\frac{dS_2}{dt} &= \lambda_1MS_1 - \lambda_3S_2 - (1-\nu)\lambda_1S_2,\\
\frac{dS_3}{dt} &= \lambda_1S_1 + (1-\nu)\lambda_1S_2 - \lambda_4S_3 - r_4S_3,\\
\frac{dS_4}{dt} &= r_4S_3 - r_1S_4 - r_2S_4,\\
\frac{dC}{dt} &= r_5C\left(1-\frac{C}{L_c}\right) - r_6C,\\
\frac{dM}{dt} &= d_1S_3 - d_2M,\\
\frac{dU_F}{dt} &= e_1(U_F+C_F) - e_2U_F - e_1U_F,\\
\frac{dC_F}{dt} &= e_2U_F - e_1C_F.
\end{aligned} \tag{1}$$

Table 1. Description of state variables and parameters used in the model.

Symbol	Description
S_1	Unaware susceptible population
S_2	Aware susceptible population
S_3	Infected population
S_4	Recovered population
C	Population of bacteria
M	Media campaigns
U_F	Uncontaminated food
C_F	Contaminated food
r_1	Natural growth rate of S_1, S_2, and S_3
r_2	Growth rate of recovered population
r_3	Waning rate of awareness
λ_1	Death rate of unaware susceptibles
λ_2	Natural death rate
λ_3	Rate at which unaware susceptibles become aware
τ	Delay parameter
ν	Efficacy of awareness programs
r_4	Human recovery rate
r_5	Net growth rate of *Listeria*
L_c	Carrying capacity of bacteria
r_6	Natural death rate of bacteria
d_1	Implementation rate of awareness programs
d_2	Diminishment rate of awareness programs
e_1	Rate of food removal
e_2	Rate of uncontaminated food removal

3. Positivity

Inspection reveals that every right-hand side is locally Lipschitz and satisfies the quasi-positivity property: the derivative of any state variable x_i is nonnegative when $x_i = 0$ (terms that could be negative are proportionate to x_i itself). Let the initial conditions be $S_1(0) \geq 0, \quad S_2(0) \geq 0, \quad S_3(0) \geq 0, \quad S_4(0) \geq 0, \quad C(0) \geq 0, \quad M(0) \geq 0, \quad U_F(0) \geq 0, \quad C_F(0) \geq 0$. We prove that the solutions remain non–negative for all $t > 0$.

i. Positivity of $S_1(t)$: from the first equation, $\frac{dS_1}{dt} = r_1N + r_2S_4 + r_3S_2 - \lambda_1S_1 - r_5M(t-\tau)S_1(t-\tau)$. Since all parameters and variables are non–negative, $\frac{dS_1}{dt} \geq -(\lambda_1 + r_5M(t-\tau))S_1$. Using the differential inequality and Gronwall's inequality, $S_1(t) \geq S_1(0)\exp\left[-\int_0^t(\lambda_1 + r_5M(s-\tau))ds\right] \geq 0$. Hence $S_1(t) \geq 0$ for all $t > 0$.

ii. Positivity of $S_2(t)$: from the first equation, $\frac{dS_2}{dt} = \lambda_1MS_1 - (\lambda_3 + (1-\nu)\lambda_1)S_2$. Thus, $\frac{dS_2}{dt} \geq -(\lambda_3 + (1-\nu)\lambda_1)S_2$. Hence, $S_2(t) \geq S_2(0)e^{-(\lambda_3+(1-\nu)\lambda_1)t} \geq 0$.

iii. Positivity of $S_3(t)$: from the first equation, $\frac{dS_3}{dt} = \lambda_1S_1 + (1-\nu)\lambda_1S_2 - (\lambda_4 + r_4)S_3$. Therefore, $\frac{dS_3}{dt} \geq -(\lambda_4 + r_4)S_3$. Thus, $S_3(t) \geq S_3(0)e^{-(\lambda_4+r_4)t} \geq 0$.

iv. Positivity of $S_4(t)$: from the first equation, $\frac{dS_4}{dt} = r_4S_3 - (r_1 + r_2)S_4$. Hence, $\frac{dS_4}{dt} \geq -(r_1 + r_2)S_4$ which gives $S_4(t) \geq S_4(0)e^{-(r_1+r_2)t} \geq 0$.

v. Positivity of $C(t)$: from the first equation, $\frac{dC}{dt} = r_5C\left(1 - \frac{C}{L_c}\right) - r_6C$. This can be written as $\frac{dC}{dt} = C\left[r_5\left(1 - \frac{C}{L_c}\right) - r_6\right]$. Hence, $C(t) = C(0)\exp\left(\int_0^t\left[r_5\left(1 - \frac{C(s)}{L_c}\right) - r_6\right]ds\right) \geq 0$.

vi. Positivity of $M(t)$: from the first equation, $\frac{dM}{dt} = d_1S_3 - d_2M \geq -d_2M$ which implies $M(t) \geq M(0)e^{-d_2t} \geq 0$.

vii. Positivity of $U_F(t)$: from the first equation, $\frac{dU_F}{dt} = e_1(U_F + C_F) - e_2U_F - e_1U_F$, this can be written as $\frac{dU_F}{dt} = e_1C_F - e_2U_F$. Thus, $\frac{dU_F}{dt} \geq -e_2U_F$ and therefore $U_F(t) \geq U_F(0)e^{-e_2t} \geq 0$.

viii. Positivity of $C_F(t)$: from the first equation, $\frac{dC_F}{dt} = e_2U_F - e_1C_F \geq -e_1C_F$, which implies $C_F(t) \geq C_F(0)e^{-e_1t} \geq 0$.

Since all state variables satisfy differential inequalities that preserve non–negativity, it follows that

$$(S_1(t), S_2(t), S_3(t), S_4(t), C(t), M(t), U_F(t), C_F(t)) \geq 0 \quad \text{for all} \quad t > 0,$$

whenever the initial conditions are non–negative. Thus, the feasible region of the system is

$$\Omega = \{(S_1, S_2, S_3, S_4, C, M, U_F, C_F) \in \mathbb{R}^8_+\}$$

and it is positively invariant.

4. Boundedness

We demonstrate that every solution that begins in Ω_0 is uniformly bounded.

4.1. Human compartments

Let $H(t) = S_1(t) + S_2(t) + S_3(t) + S_4(t)$. Summing the equations for S_i gives

$$H'(t) = r_1N + r_2S_4 + r_3S_2 - \lambda_1S_1 - r_5M(t-\tau)S_1(t-\tau) + \lambda_1MS_1 - \lambda_3S_2 - (1-\nu)\lambda_1S_2$$

$$+\lambda_1 S_1 + (1-\nu)\lambda_1 S_2 - \lambda_4 S_3 - r_4 S_3 + r_4 S_3 - r_1 S_4 - r_2 S_4,$$
$$= r_1 N - \lambda_3 S_2 - \lambda_4 S_3 - r_1 S_4 - r_5 M(t-\tau) S_1(t-\tau).$$

The simple differential inequality is obtained by using the nonnegativity of the subtraction terms.

$$H'(t) \leq r_1 N, \tag{2}$$

when eq. (2) is integrated, $H(t) \leq H(0) + r_1 N t$, consequently, this only produces linear growth. Biological restrictions are used to achieve uniform boundedness; usually, N is a constant recruitment or a function bounded by carrying capacity. A uniform bound is obtained if $r_1 N$ truly represents a bounded recruitment (or if the complete model has density-dependent mortality). The human compartments are bounded by N since N represents a fixed total human population in various modeling systems, meaning that $H(t) \leq N$ for all t.

4.2. Population of bacteria (C)

The C-equation is logistic with extra mortality: $C'(t) = r_5 C\left(1 - \frac{C}{L_c}\right) - r_6 C = C\left(r_5 - r_6 - \frac{r_5}{L_c} C\right)$. This equation is of the logistic kind. Let $r_* := r_5 - r_6$. $C(t) \to 0$ and C are bounded if $r_* \leq 0$. The carrying-capacity-like upper bound is produced by the logistic term if $r_* > 0$.

$$\limsup_{t\to\infty} C(t) \leq L_c\left(1 - \frac{r_6}{r_5}\right) \quad (\text{if } r_5 > r_6).$$

For all parameter values, $C(t)$ is therefore evenly constrained or uniformly bounded, i.e, it either falls to zero or stays below the effective carrying capacity..

4.3. Media M

Forced by S_3, the M-equation is linear in M:$M'(t) = d_1 S_3 - d_2 M \leq d_1 H(t) - d_2 M$. If $H(t)$ is bounded (e.g. $H(t) \leq N$), then comparison with the linear ODE $y' = d_1 N - d_2 y$ which yields $\limsup_{t\to\infty} M(t) \leq \frac{d_1 N}{d_2}$. Thus M is uniformly bounded.

4.4. Food compartments U_F, C_F

A linear subsystem with bounded forcing is formed by the last two equations:

$$U_F'(t) = e_1(U_F + C_F) - e_2 U_F - e_1 U_F = e_1 C_F - e_2 U_F,$$
$$C_F'(t) = e_2 U_F - e_1 C_F.$$

Since the sum yields $(U_F + C_F)'(t) = 0$, $U_F(t) + C_F(t) = U_F(0) + C_F(0) =: F_0$ is constant. Specifically, F_0 bounds both U_F and C_F. Combining the above estimates, we find that all state variables stay uniformly confined or uniformly bounded for $t \geq 0$ under biologically reasonable assumptions (fixed total human population N or density-dependent recruitment).

5. Permanence

Solutions with initial data inside Ω_0 are said to be persistent uniformly if they satisfy

$$\liminf_{t\to\infty} x_i(t) \geq \eta_i > 0,$$

for any biologically significant variable x_i, for certain positive constants η_i that are dependent on parameters but independent of initial conditions. We outline the conventional procedure for establishing permanence in systems including epidemic microorganisms.

5.1. Basic threshold for reproduction

By determining a threshold quantity $\mathscr{R}$, which is the model-dependent basic reproduction number. For the infection-bacteria subsystem, a formal next-generation derivation (linearization at DFE) yields an expression of the kind

$$\mathscr{R} = \frac{\text{creation of a new infection in a vulnerable population by a single infected person (and bacteria)}}{\text{overall rate of bacterial and infectious elimination}}.$$

The disease-free equilibrium (DFE) is represented by E_0, where $M^* = 0$, $S_3^* = 0$, $C^* = C_0$ (the bacterial steady state may be 0), and other variables at their DFE values. The model parameters determine the explicit formula for $\mathscr{R}$, which is represented symbolically as $\mathscr{R}(\lambda_1, d_1, r_4, \dots)$.

5.2. Persistence criterion

The interior of K is uniformly persistent if: (i) the semiflow generated by the system on the compact positively invariant set K (obtained from boundedness) is point-dissipative and smooth; (ii) the boundary of the interior attractor (i.e., the union of invariant sets where some epidemiological variables vanish) does not contain any internally chain transitive sets that attract nearby orbits when $\mathscr{R} > 1$; and (iii) the spectral radius of the linearization of the infection subsystem at the DFE exceeds one (equivalently $\mathscr{R} > 1$). Therefore, when $\mathscr{R} > 1$, disease and bacteria persist equally away from zero.

6. Steady State Analysis

6.1. Disease-free equilibrium (DFE)

Both the bacterial and diseased populations are zero at the disease-free equilibrium:

$$(S_1^*, S_2^*, S_3^*, S_4^*, C^*, M^*, U_F^*, C_F^*) = (S_1^0, S_2^0, 0, S_4^0, 0, M^0, U_F^0, C_F^0).$$

$\mathscr{R}_0$, the basic reproduction number is calculated as: $\mathscr{R}_0 = \dfrac{\text{New Infections}}{\text{Recoveries and Deaths}}$. The state in which there are no diseases in the population, denoted by $S_3 = 0$ and $C = 0$, is known as the disease-free equilibrium (DFE). Here $S_1'(t) = S_2'(t) = S_3'(t) = S_4'(t) = C'(t) = M'(t) = U_F'(t) = C_F'(t) = 0$.

i. Equations at DFE

To determine the DFE, we set $S_3 = 0$ and $C = 0$, and solve the system of equations:

- Equation for S_1: $0 = r_1 N + r_2 S_4 + r_3 S_2 - \lambda_1 S_1$. After rearranging, $S_1^* = \dfrac{r_1 N + r_2 S_4^* + r_3 S_2^*}{\lambda_1}$.
- Equation for S_2: $0 = \lambda_1 M S_1 - \lambda_3 S_2 - (1-\nu)\lambda_1 S_2$. After rearranging, $S_2^* = \dfrac{\lambda_1 M^* S_1^*}{\lambda_3 + (1-\nu)\lambda_1}$.
- Equation for S_3: At the DFE, $S_3 = 0$, so this equation is automatically satisfied.
- Equation for S_4: $0 = r_4 S_3 - r_1 S_4 - r_2 S_4$. Since $S_3 = 0$ at the DFE, we have, $S_4^* = 0$.
- Equation for C: $0 = r_5 C\left(1 - \dfrac{C}{L_c}\right) - r_6 C$. Since $C = 0$ at the DFE, this equation is satisfied.
- Equation for M: $0 = d_1 S_3 - d_2 M$. Since $S_3 = 0$ at the DFE, we have $M^* = 0$.
- Equation for U_F: $0 = e_1(U_F + C_F) - e_2 U_F - e_1 U_F$. After rearranging, we get $U_F^* = C_F^*$.
- Equation for C_F: $0 = e_2 U_F - e_1 C_F$. Substituting $U_F^* = C_F^*$, we get $C_F^* = \dfrac{e_2}{e_1} U_F^*$.

ii, Disease-free equilibrium point

The DFE is given by:

$$(S_1^*, S_2^*, S_3^*, S_4^*, C^*, M^*, U_F^*, C_F^*) = \left(\frac{r_1 N + r_3 S_2^*}{\lambda_1}, \frac{\lambda_1 M^* S_1^*}{\lambda_3 + (1-\nu)\lambda_1}, 0, 0, 0, 0, U_F^*, \frac{e_2}{e_1} U_F^*\right).$$

A condition devoid of infection is represented by the disease-free equilibrium (DFE), which serves as a baseline for examining the system's stability in the face of minor perturbations.

6.2. Existence of endemic equilibrium

Every population is positive at the endemic equilibrium. The eigenvalues of the Jacobian matrix computed at the endemic equilibrium are used to perform stability analysis. The steady-state of the system when the disease continues to exist in the population ($S_3 > 0$ and $C > 0$) is known as the endemic equilibrium (EE). At this state:

$$S_1'(t) = S_2'(t) = S_3'(t) = S_4'(t) = C'(t) = M'(t) = U_F'(t) = C_F'(t) = 0.$$

i. Equations at EE
We solve the system of equations by setting the time derivatives to zero in order to find the EE.
- Equation for S_1: $0 = r_1N + r_2S_4 + r_3S_2 - \lambda_1 S_1 - r_5 M S_1$. After rearranging
$$S_1^* = \frac{r_1N + r_2S_4^* + r_3S_2^*}{\lambda_1 + r_5M^*}.$$
- Equation for S_2: $0 = \lambda_1 M S_1 - \lambda_3 S_2 - (1-\nu)\lambda_1 S_2$. After rearranging, $S_2^* = \dfrac{\lambda_1 M^* S_1^*}{\lambda_3 + (1-\nu)\lambda_1}$.
- Equation for S_3: $0 = \lambda_1 S_1 + (1-\nu)\lambda_1 S_2 - \lambda_4 S_3 - r_4 S_3$. After rearranging,
$$S_3^* = \frac{\lambda_1 S_1^* + (1-\nu)\lambda_1 S_2^*}{\lambda_4 + r_4}.$$
- Equation for S_4: $0 = r_4 S_3 - r_1 S_4 - r_2 S_4$. After rearranging, $S_4^* = \dfrac{r_4 S_3^*}{r_1 + r_2}$.
- Equation for C: $0 = r_5 C\left(1 - \dfrac{C}{L_c}\right) - r_6 C$. After rearranging, $C^* = L_c\left(1 - \dfrac{r_6}{r_5}\right)$, if $r_5 > r_6$.
- Equation for M: $0 = d_1 S_3 - d_2 M$. After rearranging, $M^* = \dfrac{d_1 S_3^*}{d_2}$.
- Equation for U_F: $0 = e_1(U_F + C_F) - e_2 U_F - e_1 U_F$. After rearranging, $U_F^* = C_F^*$.
- Equation for C_F: $0 = e_2 U_F - e_1 C_F$. Substituting $U_F^* = C_F^*$ we get $C_F^* = \dfrac{e_2}{e_1} U_F^*$.

ii. Endemic equilibrium point
The endemic equilibrium (EE) is given by:

$$(S_1^*, S_2^*, S_3^*, S_4^*, C^*, M^*, U_F^*, C_F^*) = \left(\frac{r_1N + r_2S_4^* + r_3S_2^*}{\lambda_1 + r_5M^*}, \frac{\lambda_1 M^* S_1^*}{\lambda_3 + (1-\nu)\lambda_1}, \frac{\lambda_1 S_1^* + (1-\nu)\lambda_1 S_2^*}{\lambda_4 + r_4}, \frac{r_4 S_3^*}{r_1 + r_2}, L_c\left(1 - \frac{r_6}{r_5}\right), \frac{d_1 S_3^*}{d_2}, U_F^*, \frac{e_2}{e_1} U_F^*\right).$$

A situation where the disease continues to exist in the population is known as the endemic equilibrium (EE). It offers vital information about the characteristics and control of the disease.

7. Local Stability Analysis Without Delay

7.1. Jacobian matrix

Let $X = (S_1, S_2, S_3, S_4, C, M, U_F, C_F)^\top$. Now let us use partial derivatives to calculate the Jacobian matrix $J(X)$ evaluated at a general state. The following is a list of nonzero partial derivatives as rows match equations in the above order:

$$\begin{array}{llllllll}
\dfrac{\partial S_1'}{\partial S_1} = -\lambda_1 - r_5 M, & \dfrac{\partial S_1'}{\partial S_2} = r_3, & \dfrac{\partial S_1'}{\partial S_4} = r_2, & \dfrac{\partial S_1'}{\partial M} = -r_5 S_1, \\
\dfrac{\partial S_2'}{\partial S_1} = \lambda_1 M, & \dfrac{\partial S_2'}{\partial S_2} = -\lambda_3 - (1-\nu)\lambda_1, & \dfrac{\partial S_2'}{\partial M} = \lambda_1 S_1, & \dfrac{\partial S_3'}{\partial S_1} = \lambda_1, \\
\dfrac{\partial S_3'}{\partial S_2} = (1-\nu)\lambda_1, & \dfrac{\partial S_3'}{\partial S_3} = -(\lambda_4 + r_4), & \dfrac{\partial S_4'}{\partial S_3} = r_4, & \dfrac{\partial S_4'}{\partial S_4} = -(r_1 + r_2),
\end{array}$$

$$\begin{array}{llllllll} \dfrac{\partial C'}{\partial C} & = & r_5\left(1-\frac{2C}{L_c}\right)-r_6, & \dfrac{\partial M'}{\partial S_3} & = & d_1, & \dfrac{\partial M'}{\partial M} & = & -d_2, & \dfrac{\partial U_F'}{\partial U_F} & = & -e_2, \\ \dfrac{\partial U_F'}{\partial C_F} & = & e_1, & \dfrac{\partial C_F'}{\partial U_F} & = & e_2, & \dfrac{\partial C_F'}{\partial C_F} & = & -e_1. \end{array}$$

As a result, the Jacobian at any given position has a block structure.

7.2. Jacobian at the DFE

Using $S_1^*=N, S_2^*=S_3^*=S_4^*=M^*=0$ and an arbitrary C^* (either 0 or the positive bacteria equilibrium) to evaluate J at E_0. The entries that are not zero become:

$$J(E_0)=\begin{pmatrix} -\lambda_1 & r_3 & 0 & r_2 & 0 & -r_5N & 0 & 0 \\ 0 & -\lambda_3-(1-\nu)\lambda_1 & 0 & 0 & 0 & \lambda_1 N & 0 & 0 \\ \lambda_1 & (1-\nu)\lambda_1 & -(\lambda_4+r_4) & 0 & 0 & 0 & 0 & 0 \\ 0 & 0 & r_4 & -(r_1+r_2) & 0 & 0 & 0 & 0 \\ 0 & 0 & 0 & 0 & r_5\left(1-\dfrac{2C^*}{L_c}\right)-r_6 & 0 & 0 & 0 \\ 0 & 0 & d_1 & 0 & 0 & -d_2 & 0 & 0 \\ 0 & 0 & 0 & 0 & 0 & 0 & -e_2 & e_1 \\ 0 & 0 & 0 & 0 & 0 & 0 & e_2 & -e_1 \end{pmatrix}.$$

Up to permutation, the matrix is block lower-triangular; the diagonal blocks' eigenvalues make up its eigenvalues. More precisely, the spectrum separates out into: (i) Food-subsystem block $\begin{pmatrix} -e_2 & e_1 \\ e_2 & -e_1 \end{pmatrix}$ with eigenvalues 0 and $-(e_1+e_2)$. The conserved quantity $U_F+C_F=F_0$ is associated with the zero eigenvalue. (ii) The scalar eigenvalue of bacteria $\mu_C=r_5\left(1-\dfrac{2C^*}{L_c}\right)-r_6$. This reduces to $\mu_C=r_5-r_6$ for $C^*=0$ and $\mu_C=-(r_5-r_6)<0$ for the positive bacteria equilibrium $C^*=L_c\left(1-\dfrac{r_6}{r_5}\right)$. (iii) The 4×4 upper-left block represents the human/media subsystem.

7.3. Human-media 4×4 block and characteristic equation

Consider the subsystem on variables (S_1,S_2,S_3,M) with Jacobian

$$J_{hm}=\begin{pmatrix} -\lambda_1 & r_3 & 0 & -r_5N \\ 0 & -\lambda_3-(1-\nu)\lambda_1 & 0 & \lambda_1 N \\ \lambda_1 & (1-\nu)\lambda_1 & -(\lambda_4+r_4) & 0 \\ 0 & 0 & d_1 & -d_2 \end{pmatrix}.$$

$p(\xi)=\det(J_{hm}-\xi I)=0$ is the characteristic polynomial. This expands to a quartic polynomial

$$\xi^4+a_1\xi^3+a_2\xi^2+a_3\xi+a_4=0,$$

with coefficients a_i provided by symmetric combinations of the elements of J_{hm}. Here, we describe a factorization strategy rather than entirely expanding every term. The fourth row solely couples from S_3, while the second row has no coupling into S_1 or S_3. The determinant can be reduced to a product of two factors or, in many situations, to a quadratic times a quadratic by using block-elimination. We compute

$$\det(J_{hm}-\xi I)=\big(-\lambda_3-(1-\nu)\lambda_1-\xi\big)\det\begin{pmatrix} -\lambda_1-\xi & 0 & -r_5N \\ \lambda_1 & -(\lambda_4+r_4)-\xi & 0 \\ 0 & d_1 & -d_2-\xi \end{pmatrix}-\lambda_1 N\cdot\Delta(\xi),$$

where $\Delta(\xi)$ is the minor that was derived through expansion.

7.4. Local Stability Criteria (DFE)

Since the entire Jacobian at E_0 is block triangular, all block eigenvalues must have negative real portions for E_0 to be locally asymptotically stable. The following circumstances result from this: (i) Food block: eigenvalues $-(e_1+e_2)$ and 0. The conserved mass of food is represented by the simple zero eigenvalue, which has no effect on stability transverse to the invariant manifold where $U_F+C_F=F_0$. It is always true that $-(e_1+e_2)<0$ is necessary for stability transverse to that manifold. (ii) Bacteria block: needs $\mu_C<0$. This indicates that $r_5-r_6<0$ (i.e., $r_5<r_6$) for the trivial bacteria equilibrium $C^*=0$. The bacteria component is stable at a positive equilibrium if $r_5>r_6$ and the linearization about the DFE with $C^*>0$ yields $\mu_C=-(r_5-r_6)<0$. (iii) Human-media block: there must be negative real portions in each root of $p(\xi)$. This is similar to the Routh-Hurwitz inequality on the coefficients when the Routh-Hurwitz criterion is applied to the quartic polynomial. $a_1>0, a_1a_2-a_3>0, a_3(a_1a_2-a_3)-a_1^2a_4>0, a_4>0$.

8. Global Stability Analysis without Delay

We build a Lyapunov function as follows in order to examine the interior steady state's global stability:

$$V(S_1,S_2,S_3,S_4,C,M,U_F,C_F)=\alpha_1(S_1-S_1^*)^2+\alpha_2(S_2-S_2^*)^2+\alpha_3(S_3-S_3^*)^2+\alpha_4(S_4-S_4^*)^2+\alpha_5(C-C^*)^2 \\ +\alpha_6(M-M^*)^2+\alpha_7(U_F-U_F^*)^2+\alpha_8(C_F-C_F^*)^2,$$

where $\alpha_i>0$ are constants and $(S_1^*,S_2^*,S_3^*,S_4^*,C^*,M^*,U_F^*,C_F^*)$ represents the interior steady state. The time derivative of V is given by:

$$\frac{dV}{dt}=2\alpha_1(S_1-S_1^*)S_1'+2\alpha_2(S_2-S_2^*)S_2'+2\alpha_3(S_3-S_3^*)S_3'+2\alpha_4(S_4-S_4^*)S_4'+2\alpha_5(C-C^*)C' \\ +2\alpha_6(M-M^*)M'+2\alpha_7(U_F-U_F^*)U_F'+2\alpha_8(C_F-C_F^*)C_F'.$$

Substitute the model equations into $\frac{dV}{dt}$:

$$\frac{dV}{dt}=2\alpha_1(S_1-S_1^*)\left[r_1N+r_2S_4+r_3S_2-\lambda_1S_1-r_5MS_1\right]+2\alpha_2(S_2-S_2^*)\left[\lambda_1MS_1-\lambda_3S_2-(1-\nu)\lambda_1S_2\right] \\ +2\alpha_3(S_3-S_3^*)\left[\lambda_1S_1+(1-\nu)\lambda_1S_2-\lambda_4S_3-r_4S_3\right]+2\alpha_4(S_4-S_4^*)\left[r_4S_3-r_1S_4-r_2S_4\right] \\ +2\alpha_5(C-C^*)\left[r_5C\left(1-\frac{C}{L_c}\right)-r_6C\right]+2\alpha_6(M-M^*)\left[d_1S_3-d_2M\right] \\ +2\alpha_7(U_F-U_F^*)\left[e_1(U_F+C_F)-e_2U_F-e_1U_F\right]+2\alpha_8(C_F-C_F^*)\left[e_2U_F-e_1C_F\right].$$

We simplify $\frac{dV}{dt}$ and demonstrate that by selecting suitable constants $\alpha_i>0$ and applying the steady-state relations.

$$\frac{dV}{dt}<0 \quad \text{for all } (S_1,S_2,S_3,S_4,C,M,U_F,C_F)\neq(S_1^*,S_2^*,S_3^*,S_4^*,C^*,M^*,U_F^*,C_F^*).$$

The derivative $\frac{dV}{dt}$ of the Lyapunov function V is negative definite, although V itself is positive definite. As a result, the Listeriosis model's interior steady state is globally asymptotically stable.

9. Time Delay Analysis of the Model

Let $(S_1^*, S_2^*, S_3^*, S_4^*, C^*, M^*, U_F^*, C_F^*)$ represent the system's equilibrium point. We linearize the system around this equilibrium point in order to do delay analysis. Let $S_1 = S_1^* + x_1$, $S_2 = S_2^* + x_2$, $S_3 = S_3^* + x_3$, $S_4 = S_4^* + x_4$ represent minor perturbations around the equilibrium. Similarly, for C, M, U_F, and C_F. The linearized system is obtained by substituting into the system and ignoring higher order terms:

$$\begin{aligned}
x_1'(t) &= -(\lambda_1 + r_5 M^*)x_1(t) - r_5 S_1^* x_6(t-\tau),\\
x_2'(t) &= \lambda_1 M^* x_1(t) - (\lambda_3 + (1-\nu)\lambda_1)x_2(t),\\
x_3'(t) &= \lambda_1 x_1(t) + (1-\nu)\lambda_1 x_2(t) - (\lambda_4 + r_4)x_3(t),\\
x_4'(t) &= r_4 x_3(t) - (r_1 + r_2)x_4(t),\\
x_5'(t) &= r_5 C^* \left(1 - \frac{2C^*}{L_c}\right) x_5(t),\\
x_6'(t) &= d_1 x_3(t) - d_2 x_6(t),\\
x_7'(t) &= e_1(x_7 + x_8) - e_2 x_7 - e_1 x_7,\\
x_8'(t) &= e_2 x_7 - e_1 x_8.
\end{aligned} \tag{3}$$

The system's time delay is represented by the parameter τ, especially in the interaction term involving $M(t-\tau)$ and $S_1(t-\tau)$.

Let $x_i(t) = \phi_i e^{\lambda t}$ be the solution. An algebraic system of equations is obtained by substituting into the linearized system. For the delayed term, $x_6(t-\tau) = \phi_6 e^{\lambda(t-\tau)} = \phi_6 e^{-\lambda\tau} e^{\lambda t}$. As a result, the system can be expressed in matrix form as follows: $(A + Be^{-\lambda\tau})\Phi = 0$, where A' and B' are matrices representing the coefficients of the current and delayed states, respectively. The determinant must disappear for nontrivial solutions:

$$\det(A + Be^{-\lambda\tau}) = 0 \tag{4}$$

This gives the characteristic equation involving delay τ:

$$\lambda^n + a_{n-1}\lambda^{n-1} + \cdots + a_0 + (b_m\lambda^m + \cdots + b_0)e^{-\lambda\tau} = 0 \tag{5}$$

To determine stability, we look at the roots of the characteristic equation. If all of the roots' real parts are negative, the equilibrium is asymptotically stable. When there is a positive real component in at least one root, instability results. The delay (τ) may cause Hopf bifurcation when two complex conjugate roots cross the imaginary axis. Assume solutions of the type $\tilde{X}(t) = X_0 e^{\lambda t}$, where λ is a complex eigenvalue and X_0 is a constant vector. The result of substituting into the linearized system is:

$$\mathbf{A}\mathbf{X}_0 + \mathbf{B}\mathbf{X}_0 e^{-\lambda\tau} = \lambda\mathbf{X}_0,$$

where the linearization yields the matrices $\mathbf{A}$ and $\mathbf{B}$. The characteristic equation is found after simplification:

$$\det(\mathbf{A} - \lambda\mathbf{I} + \mathbf{B}e^{-\lambda\tau}) = 0.$$

10. Hopf-bifurcation Analysis of the Delay Model

Linearization around the steady state

Let the system's interior steady state be represented by:

$$(S_1^*, S_2^*, S_3^*, S_4^*, C^*, M^*, U_F^*, C_F^*).$$

By introducing small perturbations around the steady state:

$$S_1(t) = S_1^* + \tilde{S}_1(t), \quad S_2(t) = S_2^* + \tilde{S}_2(t), \quad \ldots \quad C_F(t) = C_F^* + \tilde{C}_F(t).$$

The linearized system is obtained by substituting into the model equations while keeping just linear terms:

$$\dot{\mathbf{X}}(t) = \mathbf{A}\mathbf{X}(t) + \mathbf{B}\mathbf{X}(t-\tau),$$

where $\mathbf{X}(t) = [\tilde{S}_1(t), \tilde{S}_2(t), \tilde{S}_3(t), \tilde{S}_4(t), \tilde{C}(t), \tilde{M}(t), \tilde{U}_F(t), \tilde{C}_F(t)]^T$, and $\mathbf{A}$ and $\mathbf{B}$ are constant coefficient matrices.

Let us consider a solution of the type $\tilde{\mathbf{X}}(t) = \mathbf{X}_0 e^{\lambda t}$. The linearized system can be substituted as follows: $\lambda \mathbf{X}_0 = \mathbf{A}\mathbf{X}_0 + \mathbf{B}\mathbf{X}_0 e^{-\lambda\tau}$. Simplify to obtain the characteristic equation:

$$\det(\mathbf{A} - \lambda \mathbf{I} + \mathbf{B}e^{-\lambda\tau}) = 0.$$

To analyze the Hopf bifurcation, consider $\lambda = i\omega$ (purely imaginary eigenvalues). Substituting $\lambda = i\omega$ into the characteristic equation and separating real and imaginary parts yields:

$$\begin{aligned} \text{Real Part: } & \det\left(\mathbf{A} + i\omega\mathbf{I} + \mathbf{B}e^{-i\omega\tau}\right) = 0, \\ \text{Imaginary Part: } & \det\left(\mathbf{A} + i\omega\mathbf{I} - \mathbf{B}e^{i\omega\tau}\right) = 0. \end{aligned}$$

These equations are solved for the critical delay τ_c and the corresponding ω_c. Substitute $\lambda = i\omega$ into $\mathbf{A} - \lambda\mathbf{I} + \mathbf{B}e^{-\lambda\tau}$ and solve for ω_c. Compute τ_c using:

$$\tau_c = \frac{\arg\left(\mathbf{A} + i\omega_c\mathbf{I}\right)}{\omega_c},$$

when $\tau < \tau_c$, the system is stable and the real part of λ is negative. A Hopf bifurcation occurs when two complex conjugate eigenvalues cross the imaginary axis at $\tau = \tau_c$. When $\tau > \tau_c$, the steady state loses stability and continuous oscillations occur when the real part of λ becomes positive.

11. Sensitivity Analysis

Sensitivity analysis is used to determine the relative importance of the model parameters on the disease transmission dynamics. In epidemiological models, this is usually performed with respect to the basic reproduction number R_0, since it determines whether the disease persists or dies out. The normalized forward sensitivity index of a variable R_0 with respect to a parameter p is defined as $\Upsilon_p^{R_0} = \dfrac{\partial R_0}{\partial p} \times \dfrac{p}{R_0}$. This index measures the relative change in R_0 due to a relative change in the parameter p.

i. Sensitivity with respect to infection rate λ_1: assuming the reproduction number has the form $R_0 = \dfrac{\lambda_1 S_1^*}{\lambda_4 + r_4}$, the sensitivity index with respect to λ_1 is $\Upsilon_{\lambda_1}^{R_0} = \dfrac{\partial R_0}{\partial \lambda_1}\dfrac{\lambda_1}{R_0}$. Since $\dfrac{\partial R_0}{\partial \lambda_1} = \dfrac{S_1^*}{\lambda_4 + r_4}$, we obtain $\Upsilon_{\lambda_1}^{R_0} = \dfrac{S_1^*}{\lambda_4 + r_4} \times \dfrac{\lambda_1}{R_0} = 1$. Thus, R_0 increases proportionally with λ_1.

ii. Sensitivity with respect to recovery rate r_4: $R_0 = \dfrac{\lambda_1 S_1^*}{\lambda_4 + r_4}$, differentiating with respect to r_4, we get $\dfrac{\partial R_0}{\partial r_4} = -\dfrac{\lambda_1 S_1^*}{(\lambda_4 + r_4)^2}$. Hence, $\Upsilon_{r_4}^{R_0} = \left(-\dfrac{\lambda_1 S_1^*}{(\lambda_4 + r_4)^2}\right)\dfrac{r_4}{R_0}$. After simplifying, $\Upsilon_{r_4}^{R_0} = -\dfrac{r_4}{\lambda_4 + r_4}$. This negative value indicates that increasing the recovery rate reduces the basic reproduction number.

iii. Sensitivity with respect to disease induced death rate λ_4: $\dfrac{\partial R_0}{\partial \lambda_4} = -\dfrac{\lambda_1 S_1^*}{(\lambda_4 + r_4)^2}$, therefore, $\Upsilon_{\lambda_4}^{R_0} = -\dfrac{\lambda_4}{\lambda_4 + r_4}$. Thus increasing the disease removal rate reduces the spread of infection.

iv. Sensitivity with respect to media campaign decay rate d_2: the media campaign dynamics influence the infection rate through the awareness population S_2. Increasing d_2 reduces media influence, which may increase disease transmission. The sensitivity index is $\Upsilon_{d_2}^{R_0} = \frac{\partial R_0}{\partial d_2}\frac{d_2}{R_0}$. Since increasing d_2 reduces awareness, the sensitivity index is generally positive.

From the above analysis, It may conclude that the sensitivity analysis shows that: (i) The infection rate λ_1 has the strongest positive impact on disease transmission, (ii)Increasing the recovery rate r_4 significantly reduces the spread of the disease, (iii) Higher disease removal rates λ_4 also decrease R_0, (iv) Media campaigns indirectly reduce the infection by increasing awareness among susceptible individuals. Thus, public health strategies that reduce the infection rate, increase recovery, and strengthen media awareness campaigns can significantly control the spread of Listeriosis.

12. Numerical Simulations

In this section, we verified the conclusions what we got in the above sections in terms of numerical simulations- using MATLAB.

Numerical observations:

The Figure 1 represents the time series evaluation of populations and food. Similarly, the Figure 2 represents time series evaluation of populations/food individually.

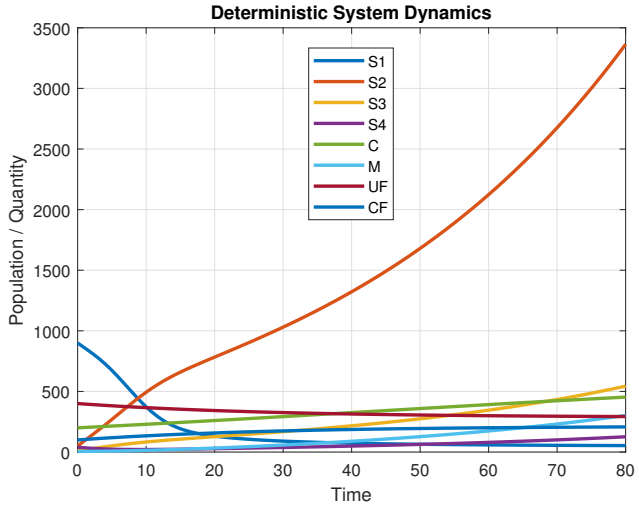

Figure 1. Time series evaluation of population with the attributes $r_1 = 0.1$; $r_2 = 0.05$; $r_3 = 0.02$; $r_4 = 0.04$; $r_5 = 0.03$; $\lambda_1 = 0.01$; $\lambda_3 = 0.015$; $\lambda_4 = 0.01$; $\alpha = 0.005$; $r_6 = 0.01$; $L_c = 1000$; $d_1 = 0.02$; $d_2 = 0.01$; $e_1 = 0.02$; $e_2 = 0.015$; $r_7 = 0.03$.

Figure 1 shows the time series projections of all populations S_1 (Unaware Susceptible), S_2(Aware Susceptible), S_3(Infected), S_4(Recovered), C(Population of bacteria), M(Media campaigns), U_F(Uncontaminated food) and C_F(Contaminated food).It clearly shows that all populations attains steady state after certain period of time and maintains the stability after some period of lag, which clearly indicates the impact of delay on the proposed system of current study.The population S_3(Infected) started at zero, but rised sharply and highly after certain period of time.New infections are intially silent but explodes highly after long period of time,as it takes more time to spread.

Figure 2 shows the time series projections of all population individually as sub figures. In sub Figure 2 S_1 (Unaware Susceptible) starts at low values and increased after some period of time. In sub Figure 2 S_2 (Aware Susceptible) starts at high values and decreased after some period of time. In sub Figure 2 S_3 (Infected) starts at high values and flattened after some period of time due to treatment or

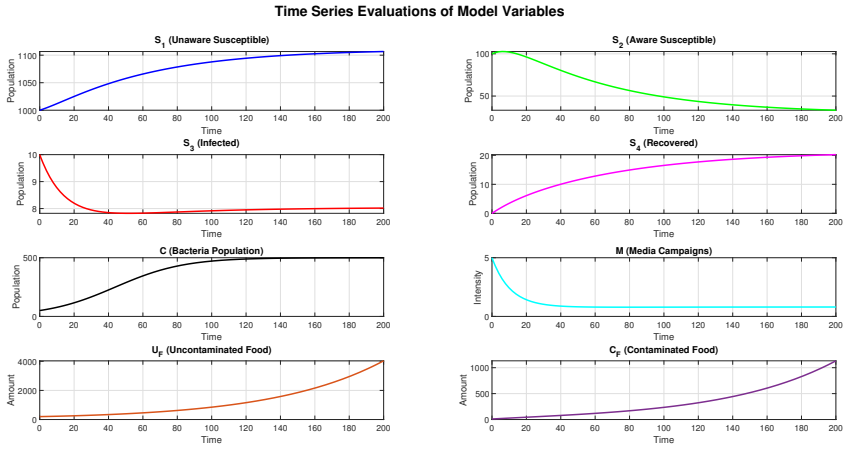

Figure 2. Time series evaluation of individual population with attributes $r_1 = 0.1$; $r_2 = 0.05$; $r_3 = 0.02$; $r_4 = 0.04$; $r_5 = 0.03$; $\lambda_1 = 0.01$; $\lambda_3 = 0.015$; $\lambda_4 = 0.01$; $\alpha = 0.005$; $r_6 = 0.01$; $L_c = 1000$; $d_1 = 0.02$; $d_2 = 0.01$; $e_1 = 0.02$; $e_2 = 0.015$; $r_7 = 0.03$.

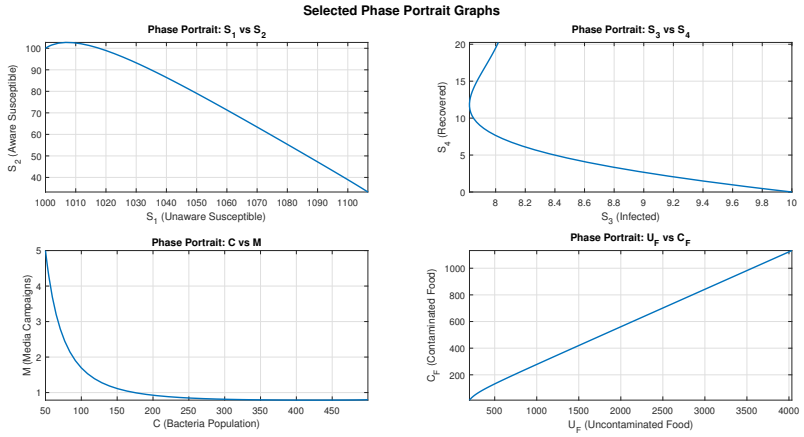

Figure 3. Phase Portrait Graphs of populations S_2, S_4, M, C_F with attributes $r_1 = 0.1$; $r_2 = 0.05$; $r_3 = 0.02$; $r_4 = 0.04$; $r_5 = 0.03$; $\lambda_1 = 0.01$; $\lambda_3 = 0.015$; $\lambda_4 = 0.01$; $\alpha = 0.005$; $r_6 = 0.01$; $L_c = 1000$; $d_1 = 0.02$; $d_2 = 0.01$; $e_1 = 0.02$; $e_2 = 0.015$; $r_7 = 0.03$.

impact of delay on system. In sub Figure 2 S_4 (Recovered) starts at zero, but rised sharply and highly after some period of time due to impactful treatment. In sub Figure 2 C(Population of bacteria) starts at low values and rised after some period of time. In sub Figure 2 M(Media Camapigns) starts with good values and attains stability after very short span of time. In sub Figure 2 U_F(Uncontaminated food) starts at zero and rised after long period of time. In sub Figure 2 C_F(Contaminated food) starts at zero and rised after very long period of time.

Figure 3 shows the following subfigures in terms of phase portraiture. (i) S_1 (Susceptible) and S_2 (Infected) have an inverse relationship; as S_1 increases, S_2 steadily decreases (a downward sloping curve); (ii) S_2 vs. S_3 (Recovered): likewise inverse; more recovered individuals are associated with fewer infected. As the bacterial population grows, multispecies levels rapidly decline, as shown by the hyperbolic-like decay of C (Bacteria Population) vs. M (Multispecies). (iv) U_1 (unconsumed food) and C_r (consumed food) have a significant linear positive relationship; as unconsumed food increases, more food is consumed, suggesting that total resources are being conserved. Biological findings show that (i) as the number of vulnerable people increases, the number of infected cases reduces (possible

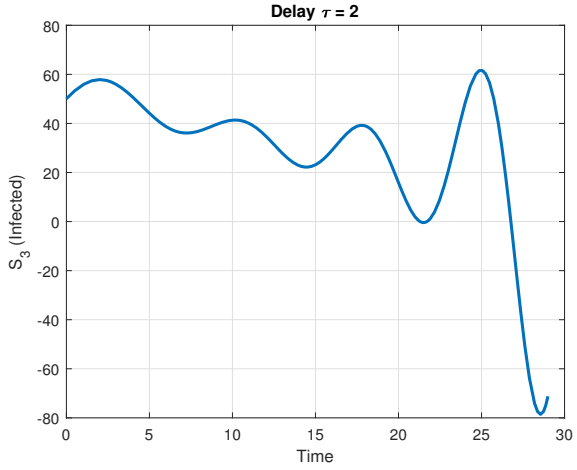

Figure 4. Time series evaluation if infected population with $\tau = 2$ and the attributes $r_1 = 0.1$; $r_2 = 0.05$; $r_3 = 0.02$; $r_4 = 0.04$; $r_5 = 0.03$; $\lambda_1 = 0.01$; $\lambda_3 = 0.015$; $\lambda_4 = 0.01$; $\alpha = 0.005$; $r_6 = 0.01$; $L_c = 1000$; $d_1 = 0.02$; $d_2 = 0.01$; $e_1 = 0.02$; $e_2 = 0.015$; $r_7 = 0.03$.

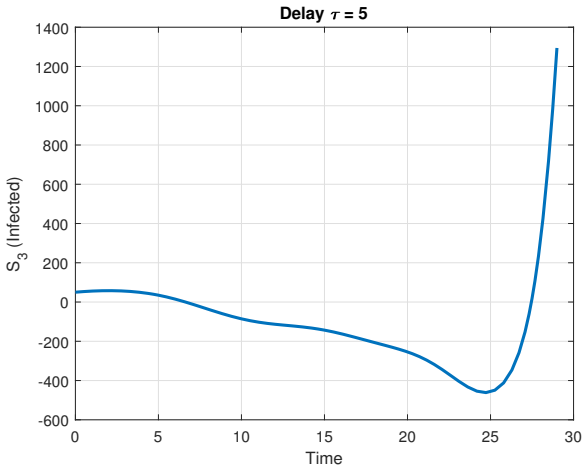

Figure 5. Time series evaluation if infected population with $\tau = 5$ and the attributes $r_1 = 0.1$; $r_2 = 0.05$; $r_3 = 0.02$; $r_4 = 0.04$; $r_5 = 0.03$; $\lambda_1 = 0.01$; $\lambda_3 = 0.015$; $\lambda_4 = 0.01$; $\alpha = 0.005$; $r_6 = 0.01$; $L_c = 1000$; $d_1 = 0.02$; $d_2 = 0.01$; $e_1 = 0.02$; $e_2 = 0.015$; $r_7 = 0.03$.

intervention influence or depletion of infection pressure). (ii) Disease progression: More persons who have recovered also have fewer infections now as immunity grows. (iii) Multispecies vs bacteria: As the bacterial burden rises, multispecies decline, suggesting ecological competition or inhibitory effects. (iv) A balance between consumed and non-consumed food implies an ecosystem's capacity to transfer resources effectively.

The time series evaluation of the infected population with time delay $\tau = 2$ is shown in Figure 4, where the infected population (S_2) exhibits damped but uneven peaks and troughs and oscillates strongly over time. Time 0˜15 shows modest oscillations at first, followed by a dramatic fall in amplitude around time 20–25. Peaks exceed +60 infected, while troughs fall below −40 (negative values could be a numerical artefact or an overshoot above the biologically possible range). The oscillations point to instability brought on by the system's delay ($\tau = 2$). When feedback is delayed ($\tau = 2$), infection dynamics become unstable. The infected population fluctuates with significant oscillations rather than stabilising. From a biological perspective, this could indicate that a delayed

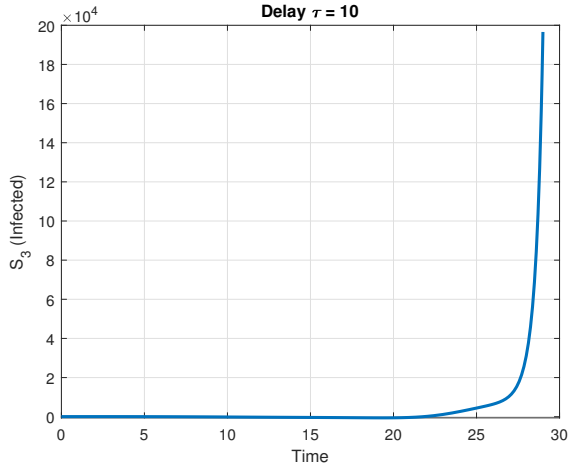

Figure 6. Time series evaluation of infected population with $\tau = 10$ and the attributes $r_1 = 0.1$; $r_2 = 0.05$; $r_3 = 0.02$; $r_4 = 0.04$; $r_5 = 0.03$; $\lambda_1 = 0.01$; $\lambda_3 = 0.015$; $\lambda_4 = 0.01$; $\alpha = 0.005$; $r_6 = 0.01$; $L_c = 1000$; $d_1 = 0.02$; $d_2 = 0.01$; $e_1 = 0.02$; $e_2 = 0.015$; $r_7 = 0.03$.

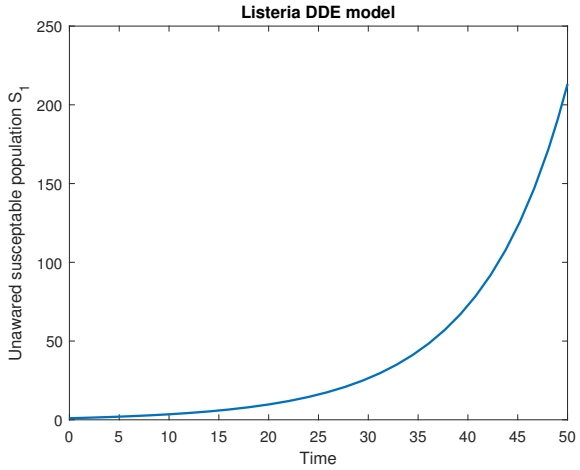

Figure 7. Time series evaluation of unawared population with attributes $r_1 = 0.1$; $r_2 = 0.05$; $r_3 = 0.02$; $r_4 = 0.04$; $r_5 = 0.03$; $\lambda_1 = 0.01$; $\lambda_3 = 0.015$; $\lambda_4 = 0.01$; $\alpha = 0.005$; $r_6 = 0.01$; $L_c = 1000$; $d_1 = 0.02$; $d_2 = 0.01$; $e_1 = 0.02$; $e_2 = 0.015$; $r_7 = 0.03$.

immune response, an incubation period, or late interventions lead to an overabundance of infections in the population. The significant oscillations might resemble epidemic waves, in which infection continuously rises and lowers until perhaps collapsing. Infection numbers that are negative are not biologically valid; instead, they suggest that the model is limited or that the parameters need to be improved.

The estimates of the infected population S_3 at various delays $\tau = 5$ and $\tau = 10$ are displayed in Figures 5 and 6, respectively. At the delay value $\tau = 5$, Figure 5 illustrates that the infected population S_3 is less affected and does not spread rapidly. Faster feedback between the illness and its spreading nature is provided by this delay setting. Partial control of outbreaks is demonstrated by the infection dynamics delay value $\tau = 5$. The infected population S_3 is more influenced, as seen in Figure 6, and at first does not spread before exploding at the delay value $\tau = 10$. Due to the fact that new infections take longer to spread, this delay value delays their spread. In infection dynamics, the delay value $\tau = 10$ shows breakout because infections "accumulate silently" during the wait, leading to an abrupt

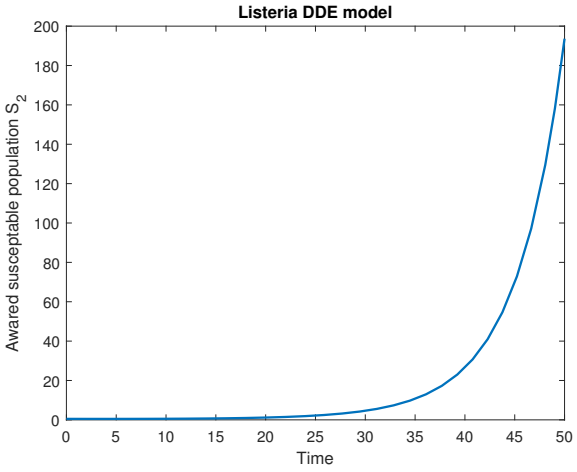

Figure 8. Time series evaluation of awared population with attributes $r_1 = 0.1$; $r_2 = 0.05$; $r_3 = 0.02$; $r_4 = 0.04$; $r_5 = 0.03$; $\lambda_1 = 0.01$; $\lambda_3 = 0.015$; $\lambda_4 = 0.01$; $\alpha = 0.005$; $r_6 = 0.01$; $L_c = 1000$; $d_1 = 0.02$; $d_2 = 0.01$; $e_1 = 0.02$; $e_2 = 0.015$; $r_7 = 0.03$.

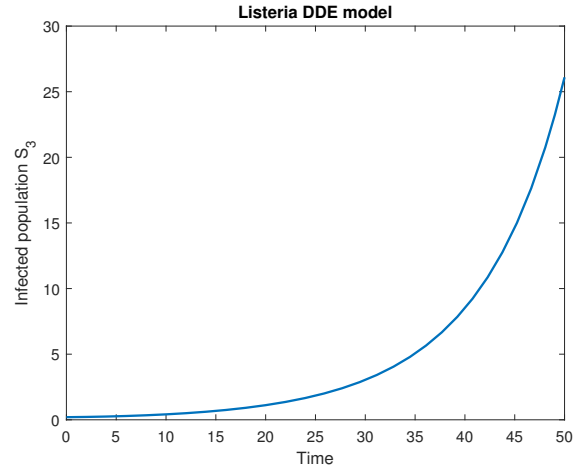

Figure 9. Time series evaluation of infected population with attributes $r_1 = 0.1$; $r_2 = 0.05$; $r_3 = 0.02$; $r_4 = 0.04$; $r_5 = 0.03$; $\lambda_1 = 0.01$; $\lambda_3 = 0.015$; $\lambda_4 = 0.01$; $\alpha = 0.005$; $r_6 = 0.01$; $L_c = 1000$; $d_1 = 0.02$; $d_2 = 0.01$; $e_1 = 0.02$; $e_2 = 0.015$; $r_7 = 0.03$.

and explosive pandemic.

The time series projections for the populations S_1, S_2, S_3, and S_4 are displayed in Figures 7 to 10, respectively. Every figure starts at zero, flattens out for a while, and then gradually increases after a given amount of time. The graph's characteristics indicate that there is a lag time before a notable and substantial increase in population. The populations' dynamics amply demonstrate the model's astounding effect of delay.

Bifurcation behaviour for r_5 between 2.2 and 4.0 is depicted in Figure 11. The system tends towards a stable fixed point (a single population value) when $r_5 < 3.0$. The first period-doubling bifurcation takes place at $r_5 \approx 3.0$. Subsequent bifurcations take place between $3.0 < r_5 < 3.453$, doubling the number of population states: period-2, period-4, period-8, and so forth. The system enters a chaotic zone at $r_5 \approx 3.57$, where population points no longer follow a straightforward repeating cycle. Before chaos returns, there are brief "windows" of periodicity (such as about $r_5 \approx 3.8$) during which momentary order returns.

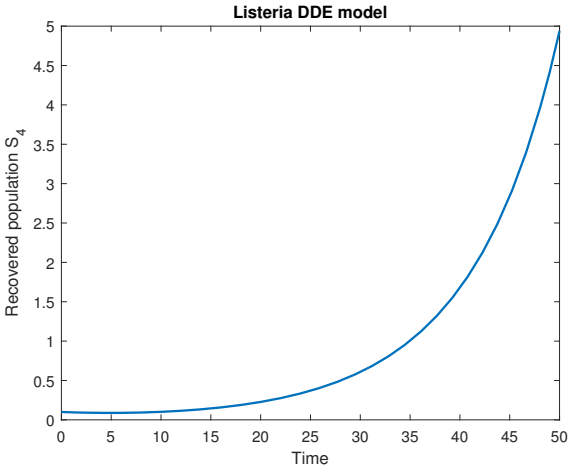

Figure 10. Time series evaluation of recovered population with attributes $r_1 = 0.1$; $r_2 = 0.05$; $r_3 = 0.02$; $r_4 = 0.04$; $r_5 = 0.03$; $\lambda_1 = 0.01$; $\lambda_3 = 0.015$; $\lambda_4 = 0.01$; $\alpha = 0.005$; $r_6 = 0.01$; $L_c = 1000$; $d_1 = 0.02$; $d_2 = 0.01$; $e_1 = 0.02$; $e_2 = 0.015$; $r_7 = 0.03$.

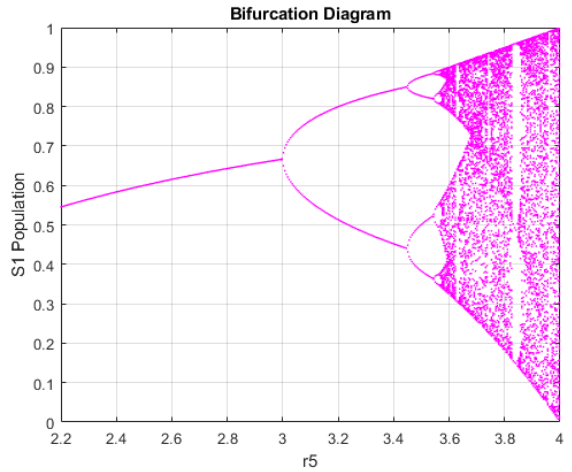

Figure 11. Bifurcation diagram with attributes $r_1 = 0.1$; $r_2 = 0.05$; $r_3 = 0.02$; $r_4 = 0.04$; $r_5 = 0.03$; $\lambda_1 = 0.01$; $\lambda_3 = 0.015$; $\lambda_4 = 0.01$; $\alpha = 0.005$; $r_6 = 0.01$; $L_c = 1000$; $d_1 = 0.02$; $d_2 = 0.01$; $e_1 = 0.02$; $e_2 = 0.015$; $r_7 = 0.03$.

The normalised population S_1 remains in the range of 0 to 1 throughout Figure 11, with the chaotic region showing the greatest spread. A sustainable population size is shown by the population stabilising at a single equilibrium for decreasing values of r_5 (growth rate). The population starts to fluctuate between two values (period-2), four, and eight as the growth rate rises. In terms of biology, this indicates that rather than stabilising, the species' population cycles seasonally or generationally. When the population reaches a crucial threshold ($r_5 \approx 3.57$), it exhibits dramatic year-to-year swings and becomes unpredictable. This illustrates how the ecosystem in the model is impacted by even minor environmental changes, leading to sporadic fluctuations in the population. In terms of ecology, there might be instances in which the system momentarily returns to stability (for instance, as a result of environmental feedback).

Bifurcation points for S_1 as a function of r_1 are indicated by the bifurcation diagram (Figure 12), which has upper, mid, and lower branches. The steady-state value of S_1 (unaware susceptible population) is shown to alter when the bifurcation parameter r_1, which is the natural growth rate for S_1,

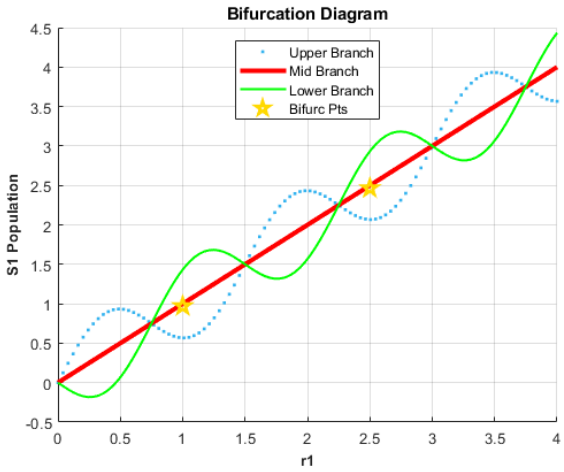

Figure 12. Bifurcation diagram with attributes $r_1 = 0.1$; $r_2 = 0.05$; $r_3 = 0.02$; $r_4 = 0.04$; $r_5 = 0.03$; $\lambda_1 = 0.01$; $\lambda_3 = 0.015$; $\lambda_4 = 0.01$; $\alpha = 0.005$; $r_6 = 0.01$; $L_c = 1000$; $d_1 = 0.02$; $d_2 = 0.01$; $e_1 = 0.02$; $e_2 = 0.015$; $r_7 = 0.03$.

varies in this bifurcation diagram. The bifurcation points—key values of r_1 where the stability or number of steady-state solutions varies—are indicated by the yellow stars. Bifurcations here take place at $r_1 = 1$ and $r_1 = 2.5$. The y-axis shows the variable S_1's corresponding steady-state value, and the x-axis shows the control parameter, r_1.

At the bifurcation points, S_1 experiences significant qualitative changes as r_1 rises. Only the lowest branch (steady-state around zero or negative, frequently ignored and biologically impractical) occurs for $r_1 < 1$. A bifurcation takes place at $r_1 \approx 1$, allowing for the emergence or merger of new solution branches (upper and lower). There are several steady states for the same value of r_1 between $r_1 \approx 1$ and $r_1 \approx 2.5$, suggesting bistability or multistability in the system. With branches merging or splitting, the number of steady states varies once more at the subsequent bifurcation ($r_1 \approx 2.5$).

Figure 12 shows areas of parameter space where, depending on the initial conditions and the nonlinearities of the system, slight variations in the growth rate r_1 can drastically modify the population dynamics and possibly cause abrupt outbreaks or elimination. Based on mathematical epidemiological models, this approach can be used to identify crucial transitions and thresholds in disease propagation or management measures.

13. Discussion and Concluding Remarks

This work presents a unified mathematical framework for understanding the spread of Listeriosis by integrating human behaviour, bacterial growth, food contamination, and media influence. By incorporating awareness-based compartments and delay effects, the model captures realistic transmission dynamics and highlights how time lags in campaigns or contamination can alter system stability. The stability and sensitivity analyses identify the key thresholds and parameters that govern both disease elimination and persistence. Overall, the study offers clear insights into how targeted interventions, timely awareness efforts, and improved food safety measures can effectively reduce the burden of Listeriosis on public health.

Limitations/future works: The proposed model employs a simplified media influence function primarily for analytical clarity and mathematical tractability. However, in real-world scenarios, the effectiveness of media-driven awareness may diminish over time due to information fatigue among the public. Additionally, the spread of misinformation through media channels can potentially weaken the impact of awareness campaigns. These aspects are not explicitly incorporated in the present model and remain an open issue that may be addressed in future research. Incorporating stochastic effects into the

present model may also consider in future works.

Supplementary Information

Author Contributions. **Kapil Toor:** Contributed towards the calculations of boundedness, positivity analysis, stability analysis. **Kalyan Das:** Designed the mathematical model and did the entire analysis with compilation.

Acknowledgements. The authors are thankful to the editors and reviewers who have supported us in improving this manuscript.

Funding. This research received no external funding.

Conflict of interest. The authors declare no conflict of interest.

Data availability. Not applicable.

References

[1] Kermack WO, McKendrick AG. A Contribution to the Mathematical Theory of Epidemics. Proceedings of the Royal Society of London Series A, Containing Papers of a Mathematical and Physical Character. 1927;115(772):700-21.
[2] Anderson RM, May RM. Population Biology of Infectious Diseases. Berlin, Heidelberg: Springer Berlin Heidelberg; 1982. doi:10.1007/978-3-642-68635-1.
[3] Van Den Driessche P, Watmough J. Reproduction numbers and sub-threshold endemic equilibria for compartmental models of disease transmission. Mathematical Biosciences. 2002 nov;180(1-2):29-48. doi:10.1016/S0025-5564(02)00108-6.
[4] Hutson V, Schmitt K. Permanence and the dynamics of biological systems. Mathematical Biosciences. 1992 sep;111(1):1-71. doi:10.1016/0025-5564(92)90078-B.
[5] Zhao XQ. Dynamical Systems in Population Biology. CMS Books in Mathematics. Cham: Springer International Publishing; 2017. doi:10.1007/978-3-319-56433-3.
[6] Allerberger F, Wagner M. Listeriosis: a resurgent foodborne infection. Clinical Microbiology and Infection. 2010 jan;16(1):16-23. doi:10.1111/j.1469-0691.2009.03109.x.
[7] Schlech WF, Acheson D. Foodborne listeriosis. Clinical Infectious Diseases. 2000 sep;31(3):770-5. doi:10.1086/314008.
[8] Africa DHRoS. National Listeria Incident Management Team; 2020.
[9] Chukwu CW, Nyabadza F. A Theoretical Model of Listeriosis Driven by Cross Contamination of Ready-to-Eat Food Products. International Journal of Mathematics and Mathematical Sciences. 2020 mar;2020:1-14. doi:10.1155/2020/9207403.
[10] Luber P, Crerar S, Dufour C, Farber J, Datta A, Todd ECD. Controlling Listeria monocytogenes in ready-to-eat foods: Working towards global scientific consensus and harmonization - Recommendations for improved prevention and control. Food Control. 2011 sep;22(9):1535-49. doi:10.1016/j.foodcont.2011.01.008.
[11] Mejlholm O, Bøknæs N, Dalgaard P. Development and validation of a stochastic model for potential growth of Listeria monocytogenes in naturally contaminated lightly preserved seafood. Food Microbiology. 2015 feb;45(PB):276-89. doi:10.1016/j.fm.2014.06.006.
[12] Ricci A, Allende A, Bolton D, Chemaly M, Davies R, Fernández Escámez PS, et al. Listeria monocytogenes contamination of ready-to-eat foods and the risk for human health in the EU. EFSA Journal. 2018 jan;16(1). doi:10.2903/j.efsa.2018.5134.
[13] Osman S, Otoo D, Sebil C. Analysis of Listeriosis Transmission Dynamics with Optimal Control. Applied Mathematics. 2020;11(07):712-37. doi:10.4236/am.2020.117048.
[14] Osman S, Makinde OD. A Mathematical Model for Coinfection of Listeriosis and Anthrax Diseases. International Journal of Mathematics and Mathematical Sciences. 2018 aug;2018:1-14. doi:10.1155/2018/1725671.
[15] Liu Y, Zhang P, Wang D, Wang B, Zhang Y, Zhang X. Prevalence and characteristics of Listeria monocytogenes in ready-to-eat chilled pot skewer products. Frontiers in Microbiology. 2025 oct;16. doi:10.3389/fmicb.2025.1681344.
[16] Viancelli A, Pagnussatt Bringhenti R, Macedo Arruda N, Manica G, Novaski Scheuermann A, Michelon W. Contamination and quantitative microbial risk assessment of commercial salami in Southern Brazil. Academia Biology. 2025 sep;3(3). doi:10.20935/acadbiol7893.
[17] Luber P, Crerar S, Dufour C, Farber J, Datta A, Todd ECD. Controlling Listeria monocytogenes in ready-to-eat foods: Working towards global scientific consensus and harmonization - Recommendations for improved prevention and control. Food Control. 2011 sep;22(9):1535-49. doi:10.1016/j.foodcont.2011.01.008.
[18] Skjerdal T, Gangsei LE, Alvseike O, Kausrud K, De Cesare A, Alexa EA, et al. Development and validation of a regression model for Listeria monocytogenes growth in roast beefs. Food Microbiology. 2021 sep;98:103770. doi:10.1016/j.fm.2021.103770.
[19] Mejlholm O, Bøknæs N, Dalgaard P. Development and validation of a stochastic model for potential growth of Listeria

monocytogenes in naturally contaminated lightly preserved seafood. Food Microbiology. 2015 feb;45(PB):276-89. doi:10.1016/j.fm.2014.06.006.

[20] Garrido V, García-Jalón I, Vitas AI, Sanaa M. Listeriosis risk assessment: Simulation modelling and "what if" scenarios applied to consumption of ready-to-eat products in a Spanish population. Food Control. 2010 mar;21(3):231-9. doi:10.1016/j.foodcont.2009.05.019.

[21] Zhou Z, An H, Li Z, Liu Y, Dong Q. Machine learning modeling for predicting growth dynamics of Listeria monocytogenes using ComBase database: A comprehensive feature engineering approach. Food Research International. 2026 apr;230:118585. doi:10.1016/j.foodres.2026.118585.

[22] Bonilla-Luque OM, Possas A, Gonzales-Barron Ú, Cadavez V, Ezzaky Y, Hussein A, et al. Controlling Listeria monocytogenes contamination in fresh goat milk cheeses: Dynamic modelling during storage. Food Control. 2025 aug;174:111194. doi:10.1016/j.foodcont.2025.111194.

[23] Fatahillah HA, Aldila D. Forward and Backward Bifurcation Analysis From an Imperfect Vaccine Efficacy Model With Saturated Treatment and Saturated Infection. Jambura Journal of Biomathematics (JJBM). 2025 jan;5(2):132-43. doi:10.37905/jjbm.v5i2.28810.

[24] Chukwu CW, Nyabadza F, Asamoah JKK. A mathematical model and optimal control for Listeriosis disease from ready-to-eat food products. International Journal of Computing Science and Mathematics. 2023;17(1):39. doi:10.1504/IJCSM.2023.130421.

[25] Alkali M, Abdullahi M, Alhassan A, Muhammad S, Zailani H. Mathematical Analysis of a Risk Structured Listeriosis Dynamics Model. Fudma Journal of Sciences. 2025 mar;9(3):302-8. doi:10.33003/fjs-2025-0903-3259.